Colloidal Clusters with Finite Binding Energies: Fractal Structure and Growth Mechanism

ARTICLE *in* LANGMUIR · APRIL 1999

Impact Factor: 4.46 · DOI: 10.1021/la981233v

4 AUTHORS:

Maria Tirado-Miranda
University of Granada
26 PUBLICATIONS **264** CITATIONS
SEE PROFILE

Artur Schmitt
University of Granada
52 PUBLICATIONS **704** CITATIONS
SEE PROFILE

Jose Callejas-Fernandez
University of Granada
68 PUBLICATIONS **786** CITATIONS
SEE PROFILE

Antonio Fernández-Barbero
Universidad de Almería
97 PUBLICATIONS **1,762** CITATIONS
SEE PROFILE

Colloidal Clusters with Finite Binding Energies: Fractal Structure and Growth Mechanism

M. Tirado-Miranda,† A. Schmitt,† J. Callejas-Fernández,† and A. Fernández-Barbero*,‡

Biocolloid and Fluid Physics Group, Department of Applied Physics, University of Granada, E-18071 Granada, Spain, and Complex Fluid Physics Group, Department of Applied Physics, University of Almería, E-04120 Almería, Spain

Received September 14, 1998. In Final Form: December 22, 1998

Surfactant molecules (SDS) adsorbed on polystyrene microspheres are usually used as stabilizing agents. Nevertheless these molecules could modify the structure of clusters and the growth kinetics in aggregation processes. In this article we present an experimental study in which direct information on the structure of the aggregates and the aggregation mechanisms are assessed by two independent methods. Static light scattering (SLS) was used to measure the fractal dimension for clusters and dynamic light scattering (DLS) was used to determine the time evolution of the cluster mass. The cluster structure and the aggregation kinetics were identified by determining the fractal dimension and the homogeneity exponent appearing in the reaction kernels. The obtained results indicate that the salt concentration alters the cluster structure and the aggregation mechanism, whereas the surfactant molecules are responsible only for the cluster structure, probably by a restructuring process within the clusters. Osmotic and elastic−steric interactions are taken into account for supporting the idea of a rearrangement process once clusters are formed. The repulsive barrier appearing at short distances (twice the surfactant layer thickness) forces the particles to be located at a certain distance, just at the minimum of the potential curve, where attractive van der Waals forces are weaker than when particles are able to keep in direct contact.

The knowledge of the stability of colloidal suspensions is of paramount importance for the development of different applications in medicine, pharmacy, water detoxification, and, of course, ecology.[1] An example of such applications is the use of small colloidal particles on which a chemical reaction is performed during water detoxification.[2] Another interesting application appears when particles are used as an optical amplifier for antigen−antibody reactions.[3]

A frequently encountered problem is the stabilization of such colloidal particles. It is well-known that small particles are generally more difficult to stabilize than big ones, just as Derjaguin−Landau−Verwey−Overbeek (DLVO) theory predicts. In most situations, stable systems are obtained by adding a surfactant to the particles.[4] An important question appearing when the stabilized systems are going to be used for subsequent aggregations is how the process kinetics and the cluster structure are affected by the previous surfactant stabilization. Several works dealing with this subject have been published in the past decade. Liu et al.[5] studied the aggregation of colloidal gold by static light scattering and high-resolution transmission electron microscopy. Aggregation was induced by adsorption of a cationic surfactant (Adgon 462, quaternary ammonium salt) onto gold particles. These molecules neutralize the particle charge and aggregate the samples. They found a dependence of the cluster fractal dimension on the amount of adsorbed surfactant, in good agreement with the theoretical predictions from the Shih−Aksay−Kikuchi (SAK) simulation model.[6] A microphotograph is also shown where a separation of about 1−2 nm between monomers is observed for clusters formed in the presence of surfactant.

An interesting article by Zhu and Napper[7] addresses the influence of temperature and salt concentration on the aggregation of polystyrene particles sterically stabilized by poly(*N*-isopropylacrylamide). A polymer containing hydrophobic moieties was introduced into the particle interfacial layers, as well as amide groups capable of H bonding with water. They found an unexpected result: the fractal dimension rose with increasing salt concentration. These observations do not agree with the predictions for diffusion-limited cluster aggregation (DLCA) or reaction-limited cluster aggregation (RLCA). They differ also from the normal restructuring process in which clusters formed under diffusion-limited conditions with a fractal dimension of about 1.7 restructure so that the fractal dimension increases to 2.1 after a sufficient time. The information about the cluster structure was obtained from the time evolution of the hydrodynamic radius during the aggregation processes. This magnitude depends not only on the structure of the clusters but also on the aggregation mechanism.[8] As the authors pointed out, their measurements were interpreted in terms of changes in cluster structure, under the principal but not always trivial assumption that the cluster mass increases linearly in

* Corresponding address: afernand@ualm.es.
† University of Granada.
‡ University of Almería.

(1) See, for example, *Colloids Surf. B* or *Adv. Colloid Interface Sci.* for application articles.

(2) Fernández-Nieves, A.; de las Nieves, F. J. *J. Non Equilib. Thermodyn.* **1998**, *23*, 45.

(3) Masuzawa, S.; Itoh, Y.; Kimura, H.; Koayashi, R.; Miauchi, C. H. *J. Immunol. Methods* **1983**, *60*, 189. Millan, J. L.; Nustad, K.; Norgaad-Pedersen, B. *Clin. Chem.* **1985**, *31*, 54. Stoll, S.; Lanet, V.; Pefferkorn, E. *J. Colloid Interface Sci.* **1993**, *157*, 302.

(4) Peula, J. M.; Fernández-Barbero, A.; Hidalgo-Álvarez, R.; de las Nieves, F. J. *Langmuir* **1997**, *13*, 3938. Peula, J. M.; Santos, R.; Forcada, J.; Hidalgo-Alvarez, R.; de las Nieves, F. J. *Langmuir* **1998**, *14*, 6377.

(5) Liu, J.; Shih, W. Y.; Sarikaya, M.; Aksay, I. A. *Phys. Rev. A: At. Mol. Opt. Phys.* **1990**, *41*, 3206.

(6) Shih, W. Y.; Aksay, I. I.; Kikuchi, R. *Phys. Rev. A: At. Mol. Opt. Phys.* **1987**, *36*, 5015.

(7) Zhu, P. W.; Napper, D. H. *Phys. Rev. E: Stat. Phys. Plasmas, Fluids, Relat. Interdiscip. Top.* **1994**, *50*, 1360.

(8) Carpineti, M.; Giglio, M. *Adv. Colloid Interface Sci.* **1990**, *46*, 13.

10.1021/la981233v CCC: $18.00
Published on Web 04/21/1999

Table 1. Characteristics of the Experimental Systems

sample	source	radius (nm)	charge density (μC/cm^2)	ccc (mM)
Lx120	Universidad de Granada	121 ± 10	−1.2 ± 0.1	394 ± 7
Lx20	Universidad del País Vasco	20 ± 5	−13 ± 2	996 ± 2
Lx90	Universidad del País Vasco	92 ± 7	−3.0 ± 0.5	437 ± 12

time, i.e., $\langle M \rangle \sim t$. In a previous paper,[9] we also used this method to measure the time evolution of the fractal dimension for the growth processes in diffusion-limited aggregation. A possibility to avoid this hypothesis is the use of a different technique to identify the aggregation mechanism directly.

In this article we present an experimental study in which information on the structure of the aggregates and the aggregation mechanisms are assessed by two independent techniques: static light scattering (SLS) to measure the fractal dimensions and dynamic light scattering (DLS) to determine the cluster mass. We will try to answer the following question: Are the surfactant molecules adsorbed on particle surfaces responsible for the cluster structure, for the aggregation mechanism, or for both. The same question will be asked for the ion concentration in the solvent.

The outline of this paper is as follows: Section I is a brief summary of the theoretical aspects of cluster structure, growth kinetics, aggregation models, and experimental techniques. The instrumental details are described in Section II. Section III describes the experimental systems. Section IV deals with the experimental results and a discussion thereof. Finally, conclusions are reported in Section V.

I. Monitoring Cluster Growth

I.A. Cluster Morphology and Kinetics of Aggregation. It is well-known that colloidal clusters exhibit a fractal structure, characterized by a fractal dimension, d_f, which is directly related to the cluster compactness. Growing clusters present an open-branched structure that shows self-similarity and is represented by a scaling law which relates the increasing radius, R, to the cluster volume $V(R)$[10]:

$$V(R) \sim R^{d_f} \tag{1}$$

On the other hand, the growth mechanism is characterized by the time evolution of the cluster-size distribution, described by the Smoluchowski rate equation. This equation provides an useful mean field approach to the kinetics and a framework to classify a wide variety of growth processes. This classification helps to distinguish between DLCA and RLCA and also to clarify the difference between aggregation and gelation.

Smoluchowski's equation[10] expresses the time evolution of the cluster-size distribution, $N(n,t)$, in terms of the reaction kernels $k(i,j)$:

$$\frac{dN(n,t)}{dt} = \frac{1}{2}\sum_{i+j=n} k(i,j)N(i,t)N(j,t) - N(n,t)\sum_{i=1}^{\infty} k(i,n)N(i,t) \tag{2}$$

This equation takes into account all pairs of collisions which may generate or deplete a given cluster size. The first term accounts for the creation of n-mers through binary collisions of i-mers and $(n-i)$-mers. The second one represents the depletion of n-mers caused by binary collisions with other clusters. $k(i,j)$ is the concentration-independent kernel that contains the physical information on the aggregation kinetics and, in general, depends on the size of the reacting clusters. Kernels are configurational and orientational averages of the reaction rates between two colliding clusters. This description is valid only for diluted suspensions, in which only collisions between two clusters are relevant.

The structure of this equation is simple, although it is difficult to know the form of the reaction kernel for a given system. Smoluchowski's equation is analytically solvable only for a few kernels; for example, constant kernel $k(i,j) = k(1, 1)$, the sum kernel $k(i,j) \sim i + j$, the product kernel $k(i,j) \sim ij$, and linear combinations thereof. Nevertheless, the fact that most coagulation kernels used in the literature are homogeneous functions of i and j (for large i and j)[11−13] makes it possible to introduce a classification scheme based on the relative probabilities of large clusters sticking to large clusters, and small clusters sticking to large clusters. When unions between small and large clusters dominate, large variations in cluster mass are discouraged, and the size distributions tend to be tightly bunched together, like a bell-shaped curve. If reactions between two large clusters dominate, the small clusters tend to be left behind and the result is a monotonically decreasing size distribution.

The dependence of homogeneous kernels on i and j at large i and/or j may be characterized by two independent exponents λ and μ, defined as follows[14]:

$$k(ai,aj) \sim a^{\lambda} k(i,j) \quad \lambda \leq 2$$

$$k(i,j) \sim i^{\mu} j^{\nu} \quad j \gg i \quad \nu \leq 1 \quad (\lambda = \mu + \nu) \tag{3}$$

Kernels with either, $\lambda > 2$ or $\nu > 1$, are unphysical, because the reactivity cannot increase faster than the cluster mass. No restrictions are imposed on μ.

The homogeneity parameter, λ, describes the tendency of a large cluster to join with another large cluster and determines the overall rate of aggregation. For $\lambda > 1$ the rate of aggregation becomes so fast that an infinite-size cluster forms in finite time and a gelation process occurs. Kernels with $\lambda \leq 1$ show nongelling behavior, i.e., an infinite cluster is formed at infinite time. Thus, the magnitude of λ allows us to distinguish between gelling and nongelling systems. Moreover, λ takes the value 0 in DLCA, and 1 in RLCA.[15]

The exponent μ establishes the rate at which big clusters bind to small clusters and its sign determines the shape of the size distribution. For $\mu < 0$ the large cluster−small cluster unions are favored and large clusters gobble up small ones, resulting in a bell-shaped size distribution

(9) Fernández-Barbero, A.; Schmitt, A.; Cabrerizo-Vílchez, M.; Martínez-García, R.; Hidalgo-Álvarez, R. *Phys. Rev. E: Stat. Phys. Plasmas, Fluids, Relat.* **1997**, *56*, 4337.

(10) Julien R.; Botet, R. *Aggregation and Fractal Aggregates*; World Scientific: River Edge, NJ, 1987.

(11) Leyvraz, F.; Tschudi, H. R. *J. Phys. A: At. Mol. Opt. Phys.* **1982**, *15*, 1951.

(12) Ziff, R. M.; Ernst, M. H.; Hendriks, E. M. *J. Phys. A: At. Mol. Opt. Phys.* **1983**, *16*, 2293.

(13) Hendriks, E. M.; Ernst, M. H.; Ziff, R. M. *J. Stat. Phys.* **1983**, *31*, 519.

(14) Van Dongen, P. G. J.; Ernst, M. H. *Phys. Rev Lett.* **1985**, *54*, 1396.

(15) Ball, R. C.; Weitz, D. A.; Witten, T. A.; Leyvraz, F. *Phys. Rev. Lett.* **1987**, *58*, 274.

because of the depletion of the smaller clusters. Kernels with negative μ appears to be good description for DLCA.[16,17] When $\mu > 0$, large cluster−large cluster unions dominate and the size distributions resulting from such kernels tend to be polydisperse, because small clusters may still exist in the presence of large ones. Thus, the size distribution decays monotonically with increasing cluster size. Kernels with positive μ properly describe the RLCA processes.[18,19]

I.B. Experimental Determination of d_f and λ. SLS allows d_f to be measured using the following relationship between the mean scattered light intensity and the scattering wave vector, $q = 4\pi/\lambda \sin(\theta/2)$, where λ is the wavelength of the light in the solvent and θ is the scattering angle[8,10]:

$$I(q) \sim q^{-d_f} \tag{4}$$

The mean scattered intensity contains information about the cluster structure in the q range, $\langle R_h\rangle^{-1} < q < R_0^{-1}$. For higher q values, the length scale corresponds to individual spheres within the cluster and the intensity is related to the particle form factor. In the low-q region, topological length correlations between clusters could be studied.

With use of this technique, typical values for the cluster fractal dimensions have been reported in the literature: 1.8 for DLCA and 2.1 for RLCA. In the intermediate regime, a continuous variation of the fractal dimension between these two values has also been observed.[8]

On the other hand, the homogeneity exponent λ may be determined from the evolution of the number average mean cluster-size, $\langle n_n\rangle = M_1/M_0$, where $M_i = \Sigma n^i N_n$ is the ith-order moment of the size distribution. For DLCA a linear increase with time is expected for long aggregation time, $\lim_{t\to\infty}\langle n_n\rangle(t) \sim t$. In RLCA an exponential behavior is predicted, $\lim_{t\to\infty}\langle n_n\rangle(t) \sim e^{\alpha t}$, where α is a fitting constant. In an intermediate regimen where the aggregation is not totally controlled by diffusion or repulsion, the number-average mean cluster size increases describing a power law in time with the exponent related to parameter λ:

$$\lim_{t\to\infty}\langle n_n\rangle(t) \sim t^{1/(1-\lambda)} \qquad 0 \le \lambda < 1 \tag{5}$$

The mean mass for fractal clusters may be derived from the mean hydrodynamic radius, $\langle R_h\rangle(t)$, once the fractal dimension is known:

$$\langle M\rangle = m_o\left(\frac{\langle R_h\rangle}{R_o}\right)^{d_f} \tag{6}$$

In this equation m_0 and R_0 are the monomer mass and radius, respectively. From this magnitude, the number-average mean cluster size is easily calculated by dividing the mean cluster mass by the monomer mass, $\langle n_n\rangle = \langle M\rangle/m_0$.

To measure the hydrodynamic radius, the scattered intensity autocorrelation function may be determined from the product of photon counts at time t and time $t + \tau$ such that $G(\tau) = \langle I(t)I(t + \tau)\rangle$. The normalized intensity autocorrelation function $g^{int}(\tau)$ given by[20]

$$g^{int}(\tau) = \frac{\langle I(t)I(t+\tau)\rangle}{\langle I(t)I(t)\rangle} \tag{7}$$

is then calculated and converted into the scattered field autocorrelation function by the aid of the Siegert relationship:

$$g^{int}(\tau) = 1 + C\,|g^{field}(\tau)|^2 \tag{8}$$

where C is a constant that depends on the optics of the instrument. Information on the cluster-size distribution is obtained from the fitting coefficient of the expanded logarithm of the field autocorrelation function:[21,22]

$$\ln g^{field}(\tau) = -\mu_1\tau + \mu_2\left(\frac{\tau^2}{2}\right) + \mu_3\left(\frac{\tau^3}{3!}\right) + \ldots \tag{9}$$

This method is called cumulant analysis and has been widely used for dynamic light-scattering data analysis. For polydisperse systems the first cumulant, μ_1, is related to the mean particle diffusion coefficient by $\mu_1 = \langle D\rangle q^2$. Once the mean particle diffusion coefficient determined, the mean hydrodynamic size may be calculated using the Stokes−Einstein relationship.

II. Instrumental Details

The light-scattering experiments presented in this article were performed using a slightly modified Malvern 4700 System (UK) working with a 488-nm-wavelength argon laser. Aggregation was monitored simultaneously by DLS and SLS. The scattered intensity autocorrelation functions were determined at different times during aggregations and registered by the same computer that controls the instrument. The scattering angle was set to 60° (the influence of the scattering angle will be presented in the Results Section). Data analysis was performed using our own computer programs. In this way the mean hydrodynamic radius was obtained as a function of time. For every SLS experiment, the photomultiplier arm was previously located at the reference position to set the 0 angle. After that, the mean scattered intensity was obtained for different angles in the range 20°−140°. When the final structure of the clusters was totally established, the mean intensity $I(q)$ showed an asymptotic time-independent behavior as predicted theoretically. From this asymptotic curve, the fractal dimensions were determined.

III. Experimental Systems

Three systems of spherical polystyrene particles were used for the aggregation experiments. Lx120 is an aqueous suspension of charged surfactant-free microspheres with a radius of 121 nm. The negative particle charge arises from sulfate groups on the surface. Lx20 is also an aqueous system of microspheres with a radius of 20 nm. These particles were synthesized by emulsion polymerization of butyl acrylate and styrene, using sodium dodecyl sulfate (SDS) and $NHCO_3$ as emulsifier and buffer, respectively. The particles were stabilized by the surfactant molecule, SDS, adhered on the particle surface. The third system was a latex with 92 nm of radius. Table 1 summarizes some characteristics of the experimental systems.

(16) Fernández-Barbero, A.; Cabrerizo-Vílchez, M.; Martínez-García, R.; Hidalgo-Álvarez, R. *Phys. Rev. E: Stat. Phys., Plasmas, Fluids, Relat. Interdiscip. Top.* **1996**, *53*, 4981.
(17) Fernández-Barbero, A.; Schmitt, A.; Cabrerizo-Vílchez, M.; Martínez-García, R. *Physica A* **1996**, *230*, 53.
(18) Broide, M. L.; Cohen, R. J. *J. Colloid Interface Sci.* **1992**, *153*, 493.
(19) Carpineti, M.; Ferri, F.; Giglio, M.; Paganini, E.; Perini, U. *Phys. Rev. A: At. Mol. Opt.Phys.* **1990**, *42*, 7347.
(20) Pecora, R. *Dynamic Light Scattering*; Pecora, R., Ed.; Plenum Press: New York, 1985.
(21) Koppel, D. E. *J. Chem. Phys.* **1972**, *57*, 4814.
(22) Brown, J. C.; Pusey, P. N. *J. Chem. Phys.* **1975**, *62*, 1136.

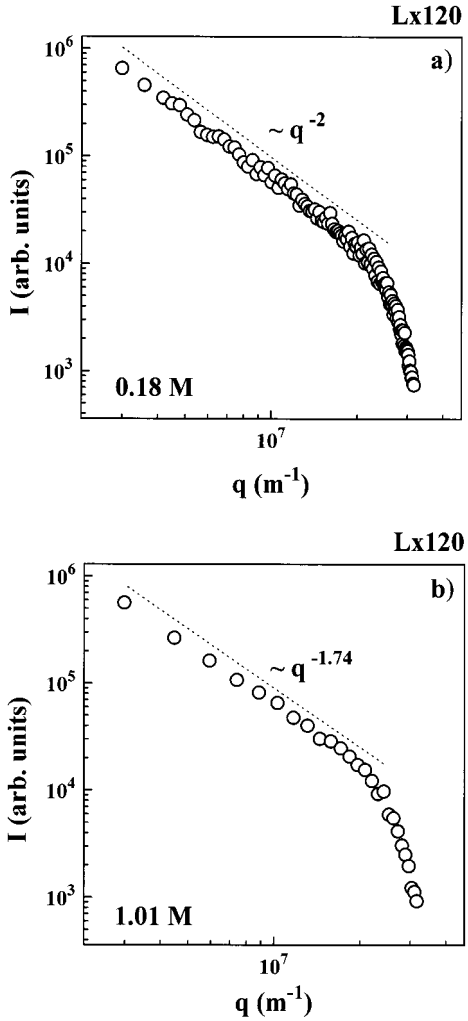

Figure 1. SLS measurements for sample Lx120: (a) aggregating at low-salt concentration (0.18 M KBr) and (b) at high-salt concentration (1.01 M KBr).

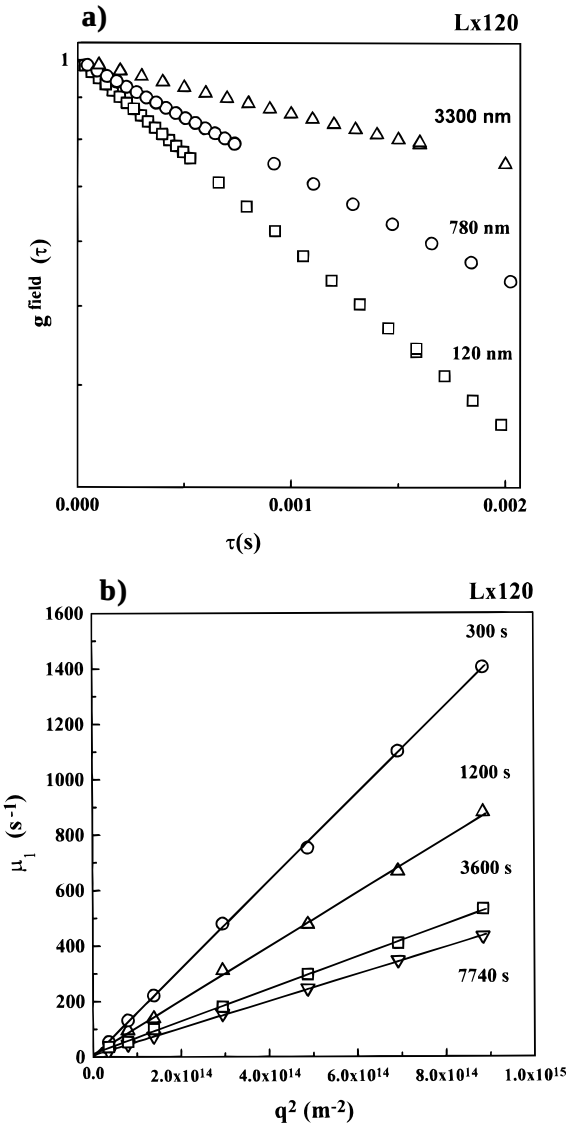

Figure 2. (a) Field autocorrelation function for different aggregation times. (b) Angular dependence of the first cumulant at different aggregation stages.

Particle size was measured by transmission electron microscopy, and surface charge densities were obtained by potentiometric and conductometric titrations. The stability was estimated by determining the critical coagulation concentration (ccc) from the time evolution of the scattered intensity.

Samples were cleaned by dialysis and serum replacement. Sonication was applied before aggregations to ensure monodisperse initial conditions. Aggregation was induced adding KBr (Merck, Analytical Grade) to the stable samples. The temperature was always set to (25 ± 1)°C with the aid of an external water thermostat.

IV. Results and Discussion

IV.A. Aggregation of Bare Particles (Lx120). Fractal dimensions of clusters in coagulated Lx120 samples were determined by SLS. Figure 1 shows the long-time asymptotic $I(q)$ curves corresponding to two different processes. The first one (Figure 1a) was induced at 0.18 M (well below the ccc) and the second one (Figure 1b) at 1.01 M KBr (well above the ccc). From the slopes at low q values, the fractal dimensions were obtained to be 2.00 ± 0.07 and 1.74 ± 0.02, respectively. The first one falls within the range commonly accepted for clusters formed under the influence of repulsive forces (RLCA), and the second one falls within the range expected for structures growing by cluster diffusion (DLCA).[8] The dropoff, observed at higher q values, corresponds to the form factor of individual particles within the clusters and does not contain information about the cluster structure.

The hydrodynamic radius was determined from the intensity autocorrelation function using cumulant analysis. Figure 2a is a typical plot showing the normalized field autocorrelation function for several aggregation stages of sample Lx120 under DLCA conditions. The mean diffusion coefficients are determined by fitting straight lines to the experimental curves at low correlation times. The slopes decrease indicating that the diffusion coefficient also decreases as the mean size increases during aggregation. Finally, the mean hydrodynamic radius is calculated by using the Einstein−Stokes relationship.

The angular dependence of the first cumulant was studied for different aggregation times to test the proper determination of the hydrodynamic radius. In fact, the interpretation of the first cumulant as the mean coefficient diffusion is based on the linear relation between the first cumulant and the square of the scattering vector, $\mu_1 = \langle D \rangle q^2$. Figure 2b shows μ_1 as a function of q^2 at several aggregation times for an aggregating Lx120 sample in DLCA conditions. In each case, the predicted linear relation is observed. The slopes contain the mean diffusion

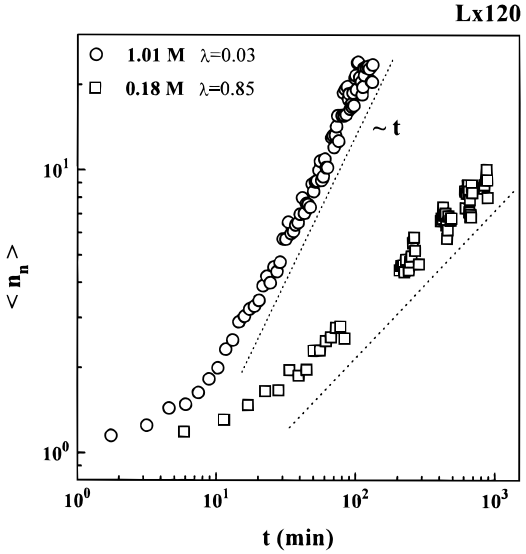

Figure 3. Number-average mean cluster size for sample Lx120. The exponent λ is determined from the slopes.

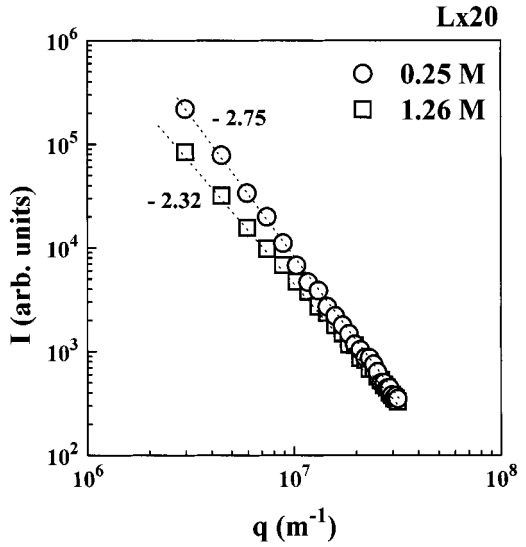

Figure 4. SLS measurements for sample Lx20. The slopes depend on the salt concentration, which indicates changes in the fractal structures.

coefficient which clearly decreases for increasing time as aggregates grow.

From the mean hydrodynamic radius and the measured fractal dimension, the mean cluster mass, $\langle M \rangle$, was determined using eq 6, and therefrom, the number-average mean cluster size calculated as $\langle n_n \rangle = \langle M \rangle / m_0$. Figure 3 shows the results for system Lx120 aggregated at 0.18 and 1.01 M KBr. It may be observed that the number-average mean cluster-size scales at long times describing a power law in time, as predicted by theory (eq 5). The slopes are related to λ, obtaining 0.85 ± 0.10 and 0.03 ± 0.06, respectively (also plotted in Figure 7 for comparison with the Lx20 system). At low-salt concentration the homogeneity exponent is close to 1 and thus the process is mainly controlled by the repulsion between clusters. For the highest ionic concentration, 1.01 M, the exponent λ is close to 0 and thus, the clusters form bonds after a pure diffusion process (DLCA). The $\langle n_n \rangle$ curves already scale for very small clusters, and so eq 5 is suitable for describing the aggregation process for almost the entire process; despite this prediction it is strictly valid for very long times. The same behavior was previously found for

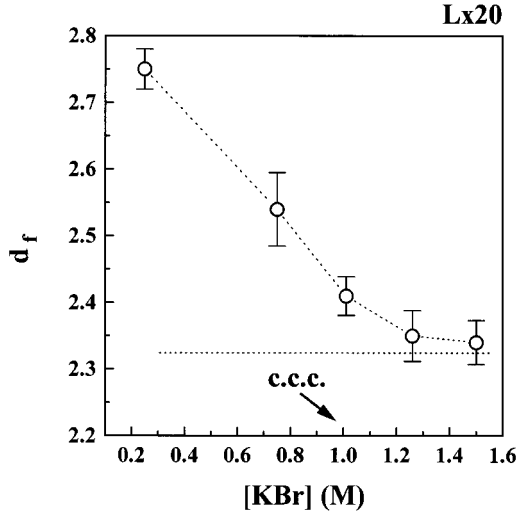

Figure 5. Fractal dimensions as a function of the salt concentration for the surfactant-covered particles, Lx20.

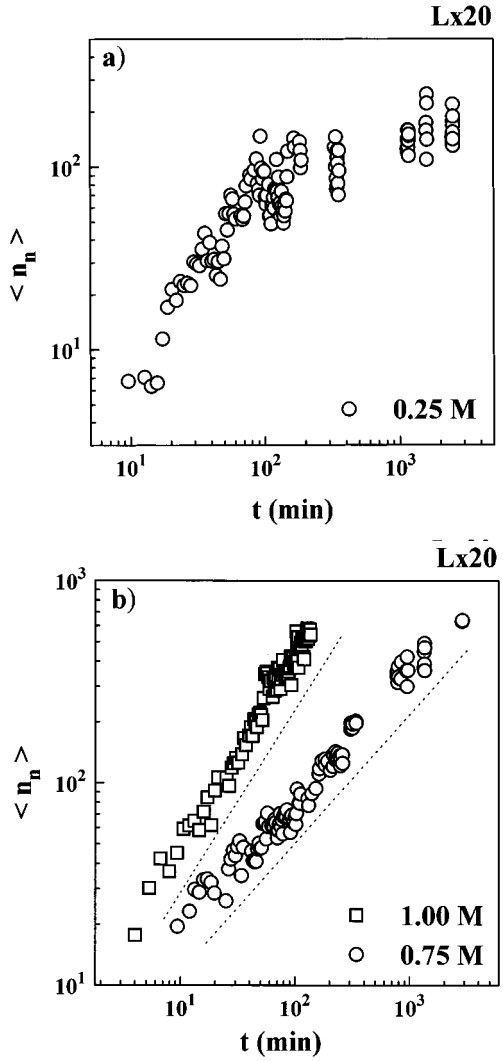

Figure 6. Number-average mean cluster size for the Lx20 particles at different salt concentrations.

the number-average mean cluster size using single-cluster light scattering.[16,17]

No exponential behavior was observed. Curves always rise describing a power law in time. Discrepancies on this subject between results from different authors keeps this discussion alive. Some RLCA experiments found that the

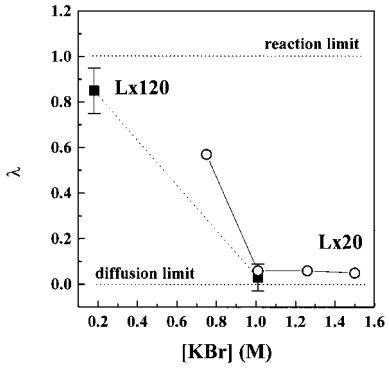

Figure 7. Homogeneity exponent λ as a function of salt concentration for bare and surfactant-covered particles.

hydrodynamic radius grows exponentially in time.[23−24] Values of λ in the range 0.8−1.0, obtained from power law in time, are also reported,[25,26] although other authors[27−31] found $\lambda \approx 1/2$ from power law curves. Meakin and Family[32] have also shown that values of λ in RLCA simulations depend critically on the rate-limiting step and thus, some models could lead to $\lambda \approx 1$, whereas others lead to $\lambda \approx 1/2$. Broide et al.[27] suggested that discrepancies could occur because the monomers they used were 10 to 100 times larger than those used in most RLCA experiments. We tried to answer this question and no correlation between monomer size and λ was found in the studied size range. The values of λ were *0.85 ± 0.10*, *0.21 ± 0.03*, and *0.57 ± 0.04* for systems with a monomer size of 121, 92, and 20 nm in radius, respectively (see Table 1). The largest value of λ corresponds to the largest monomer size. For the smallest particles, λ decreases to a value similar to that reported by Broide despite the size being 10 times smaller. Differences in the obtained values could be related to the difficulty to reproduce the same repulsion conditions between the particles which depends not only on the added salt but also on the particle's surface characteristics.

IV.B. Aggregation of Surfactant-Coated Particles (Lx20). Similar experiments were performed for the system Lx20, stabilized by SDS. Aggregations were carried out at 0.25, 0.75, 1.01, 1.26, and 1.50 M KBr. These experimental conditions cover a wide range of concentrations above the ccc, where the electric double layers of the particles are totally screened, and below the ccc, for which the interaction between particles is controlled by the amount of added salt. Figure 4 shows the mean scattered intensity as a function of the scattering wave vector for two extreme ionic concentrations. The different slopes indicate that the fractal density or cluster compactness changes with the strength of the particle interaction. The fractal dimensions are plotted as a function of the salt concentration in Figure 5. At low ionic concentration (0.25 M) the fractal dimension is fairly high (close to the space dimension), whereas at high concentrations (1.26 M) the value decreases and tends to stabilize. Despite the fact that the trend agrees with the expected crossover from RLCA to DLCA, the measured values are far from the ones normally obtained under pure reaction or diffusion conditions (as obtained for Lx120).

At this stage, an interesting question appears: Is the change of the cluster compactness in the presence of surfactant a consequence of a different aggregation mechanism? To answer this question, the exponent λ was measured for each experimental case. Figure 6 shows the number-average mean cluster size, $\langle n_n \rangle$ as a function of the time. For 0.25 M (Figure 6a) no power law was found, and therefore, the measurement of λ was not possible. This result suggests that reversible flocculation is being observed. For 0.75−1.50 M (Figure 6b), the curves scale at long time as predicted by eq 5, describing a power law in time. From the slopes, the exponents λ were determined and plotted in Figure 7. λ is close to 0 for high ionic concentrations, which indicates that the aggregation is diffusion controlled. Therefore, we may conclude that the movement of particles before binding is not responsible for the high cluster compactness ($d_f \approx 2.35$). At lower ionic concentrations, an increase in the homogeneity exponent indicates that interaction is present.

Summarizing, fractal dimensions are larger in the presence of surfactant molecules. Nevertheless, the aggregation mechanism has not been altered. Only when the ionic concentration is modified, the aggregation mechanism changes. This indicates that only the long-range electrostatic interaction is responsible for the aggregation mechanism, whereas surfactant molecules directly modify the cluster structure. So, only differences in the particle interaction at short distances should be considered in the model for explaining our experimental results.

Because SDS molecules are adsorbed on the particle surface, a steric barrier appears which prevents particles coming into contact. Vincent et al.[33] found that the stability of polymer colloids with polyelectrolytes or ionic surfactants adsorbed on the particle surface is also due to important steric effects. Thus, an osmotic repulsive potential and an elastic−steric repulsive potential should be added to the classical DLVO contributions, i.e., the Coulombian repulsive potential and the London−van der Waals attractive potential. A new force balance has to be considered: now, not only the electrostatic force but also the steric force compete against the van der Waals attractive force, resulting, under certain conditions, in a strong repulsion barrier which impedes tight unions.

For polymeric chains that cover the particle surface with an average thickness δ, an osmotic effect appears when particle surfaces are closer than a distance 2δ. The osmotic pressure of the solvent in the overlap zone will be less than that at external regions, which gives rise to a driving force for the spontaneous flow of solvent into the overlap zone, which pushes the particles apart.[34] In that case, the osmotic repulsive potential may be expressed as:

$$V_{osm} = \frac{4\pi a}{\nu}\phi^2\left(\frac{1}{2} - \chi\right)\delta^2\left[\left(\frac{H}{2\delta}\right) - \frac{1}{4} - \ln\left(\frac{H}{\delta}\right)\right] \quad (10)$$

where ν is the molecular volume of the solvent, ϕ is the effective volume fraction of segments in the adsorbed layer, and χ is the Flory−Huggins solvency parameter.

(23) Aubert, C.; Cannel, D. S. *Phys. Rev. Lett.* **1986**, *56*, 738.
(24) Bolle, G.; Cametti, C.; Codastefano, P.; Tartaglia, P. *Phys. Rev. A: At. Mol. Opt. Phys.* **1987**, *35*, 837.
(25) Martin, J. E. *Phys. Rev. A: At. Mol. Opt. Phys.* **1987**, *36*, 3415.
(26) Rarity, J. G.; Seabrook, R. N.; Carr, R. J. G. *Proc. R. Soc. London, Ser. A* **1989**, *423*, 89.
(27) Broide, M. L.; Cohen, R. J. *Phys. Rev. Lett.* **1990**, *64*, 2026.
(28) Asnaghi, D.; Carpineti, M.; Giglio, M.; Sozzi, M. *Phys. Rev. A: At. Mol. Opt. Phys.* **1992**, *45*, 1018.
(29) Von Schulthess, G. K.; Benedek, G. B.; DeBlois, R. W. *Macromolecules* **1980**, *13*, 939.
(30) Wilcoxon, J. P.; Martin, J. E.; Schaefer, D. W. *Phys. Rev A: At. Mol. Opt. Phys.* **1989**, *39*, 2675.
(31) Olivier, B. J.; Sorensen, C. M. *J. Colloid Interface Sci.* **1990**, *134*, 139.
(32) Meakin, P.; Family, F. *Phys. Rev. A: At. Mol. Opt. Phys.* **1988**, *38*, 2110.
(33) Vincent, B.; Edwards, J.; Emment, S.; Jones, A. *Colloids Surf.* **1986**, *18*, 261.
(34) Fischer, E. W. Z. Z. *Polymer* **1958**, *160*, 120.

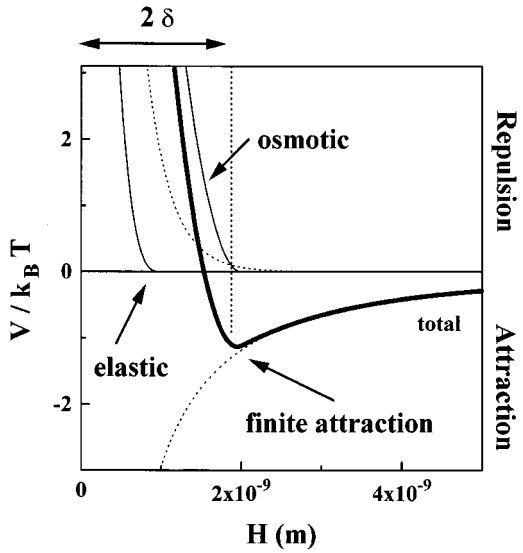

Figure 8. Total interaction potential between monomers, including steric forces, responsible for rearrangement within the clusters. The finite value for the potential in the attractive region makes the interaction weaker than for bare particles. Dashed curves represent the classical DLVO potentials.

Another effect appears when some of the polymer molecules are forced to undergo elastic compression, which corresponds to a net loss in configuration entropy. This effect gives rise to a repulsive potential related to the restriction of movement of the coils extended toward the solvent. This elastic−steric repulsion is given as:

$$V_{\text{elas}} = \left(\frac{2\pi a}{M_w}\phi\delta^2\rho_{\text{pol}}\right)\left(\frac{H}{\delta}\ln\left[\frac{H}{\delta}\left(\frac{3 - H/\delta}{2}\right)^2\right] - 6\ln\left[\frac{3 - H/\delta}{2}\right] + 3\left(1 + \frac{H}{\delta}\right)\right) \quad (11)$$

where ρ_{pol} and M_w are the density and molecular weight of the adsorbed polymer. An additivity assumption (as made in this work) is usually used for calculating the net interaction potential. Nevertheless, this hypothesis has been questioned by Einarson et al.,[35] who claim that the classical electrostatic repulsion and the steric contribution are not totally independent.

Calculations were performed for Lx120 particles using the classical DLVO interactions.[36] The diffuse potential was estimated from electrophoretic mobility measurements to be ≈20 mV. The Hamaker constant was used as a fitting parameter, obtaining 0.24×10^{-20} J at 1.01 M KBr. The discrepancy between this value and the theoretical one, calculated by the Lifschitz theory,[37] may be corrected by taking into account a shift of the reference plane for the repulsive energy outward to a distance corresponding to the thickness of the Stern layer (effect of ion size) and the increase of the diffusion coefficient caused by hydrodynamic interactions.[36] The classical interacting potential, valid for the Lx120 particles, vanishes at large distances and keeps particles tightly bound at very short distances.

The interacting potential for Lx20 particles was calculated including eqs 10 and 11 in order to account for the influence of the adsorbed surfactant. Figure 8 shows each contribution and the total interaction potential between two particles as a function of particle distance. At short distances, the osmotic component dominates over all repulsive forces and determines the behavior of the total interaction potential. At large particle distances, the potential vanishes and so, these new interactions have no influence on the movement of the particles. However, at short distances, the additional repulsive force separates the particles and locates them at a certain distance. A minimum in the total interaction potential curve appears at a distance ≈2δ. This indicates that stable unions are formed (the interaction is attractive), although the strength of the attractive force is not too large. Thus, the bonds are formed under a finite attractive interaction. This fact allows us to think about a model in which rearrangement of the monomers within the clusters should be responsible for the high degree of compactness, despite of the aggregation process being dominated by cluster diffusion.

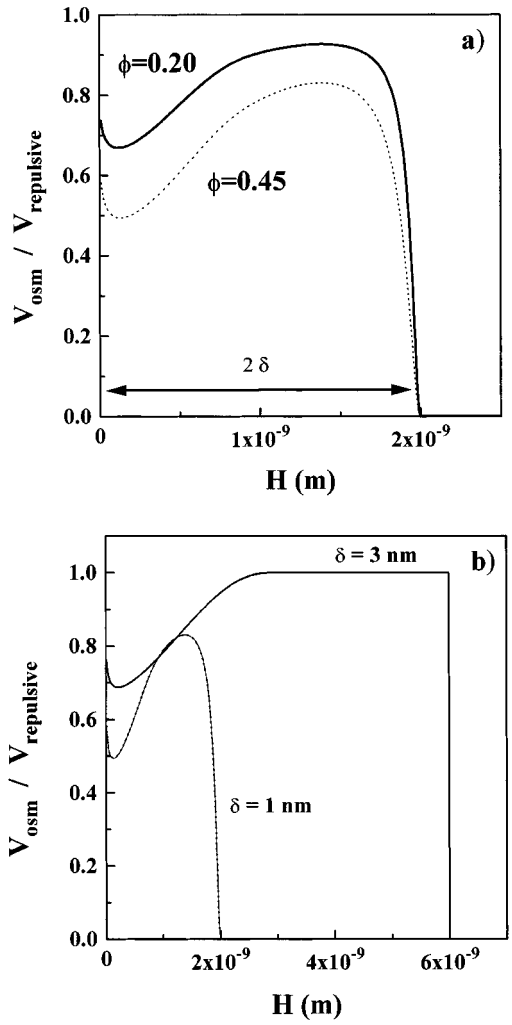

Figure 9. Osmotic interaction compared with the total repulsive barrier. Influence of (a) the effective volume fraction, ϕ, and (b) thickness of the adsorbed polymer, δ, are shown.

For calculating the steric contributions plotted in Figure 8, the Flory−Huggins solvency parameter was set at $\chi = 0.45$ (generally accepted for SDS) and the volume fraction occupied by surfactant segments was $\Phi = 0.25$. The molecular weight for SDS is 288.4 g/mol. The average thickness of the surfactant coils was $\delta = 1$ nm. This value

(35) Einarson, M. B.; Berg, J. C. *J. Colloid Interface Sci.* **1993**, *155*, 165.

(36) The method is described in: Fernández-Barbero, A.; Martín-Rodriguez, A.; Callejas-Fernández, J.; Hidalgo-Álvarez, R. *J. Colloid Interface Sci.* **1994**, *162*, 257. See also ref 4.

(37) Prieve, D. C.; Russel, W. B. *J. Colloid Interface Sci.* **1988**, *125*, 1.

is quite reasonable as pointed out by Zhao and Brown.[38] They adsorbed SDS on polystyrene particles, measuring a thickness of 1−2 nm. See also ref 5, previously mentioned in the Introduction. The diffuse potential was estimated to be ≈50 mV from the electrophoretic mobility of $(3.8 \pm 0.2) \times 10^{-8}$ m^2 V^{-1} s^{-1}.The Hamaker constant used was 1.0×10^{-20} J.

Although the values of χ, Φ, and δ determine the steric contributions, the repulsive potential barrier at short distances is guaranteed for a wide range of these parameters, so the exact value of this parameter is not critical for our explanation. The osmotic force dominates over the rest of the repulsive forces and controls the repulsive contribution which competes against the van der Waals force. Figure 9a shows the ratio between the osmotic potential and the total repulsive potential (electrostatic, osmotic, and elastic−steric). This rate is ≈0.8 in the range of distances between δ and 2δ, which confirms that the osmotic force controls the repulsive barrier. For a distance smaller than δ, the elastic force becomes relevant and the plotted rate decreases. It can be seen that a different value for the effective volume fraction of segments in the adsorbed layer, Φ, does not change the qualitative behavior of the interaction potential. The effect of the adsorbed polymer layer thickness, δ, is shown in Figure 9b.

V. Conclusions

The effect of adsorbed surfactant molecules on the structure of clusters from aggregated polystyrene microspheres was studied. Fractal dimensions are larger in the presence of surfactant molecules than with bare particles. Nevertheless, the aggregation mechanism is not altered. Only when ionic concentration is modified, the aggregation mechanisms change. This means that the electrostatic interaction is responsible for the aggregation mechanism, whereas surfactant molecules directly modify the cluster structure. Thus, differences in the particle interaction at short distances only need to be considered for the interpretation of the experimental results.

Osmotic and elastic−steric interactions were used for supporting the idea of a rearrangement process once the clusters are formed. The repulsive barrier appearing at short distances (twice the surfactant layer thickness), forces the particles to be located at a certain distance, just at the minimum of the potential curve, where attractive van der Waals forces are weaker than for the case in which particles are able to join completely. In this last case, the joints are so strong that monomers seem to be "frozen" and movement is forbidden. So, the structure is preserved. When particle attractions are weaker, monomer rearrangements are possible because of the steric repulsive force, and the clusters become more compact.

Acknowledgment. This work was supported by the CICYT-Spain, Projects MAT97-1024 and MAT96-1035-C03-02. We thank the "Grupo de Ingeniería Química de la Universidad del País Vasco" for kindly supplying Lx20 and Lx90 particles. We also wish to express gratitude to Manuel Quesada for latex particle characterization.

LA981233V

(38) Zhao, J.; Brown, W. *J. Phys. Chem.* **1995**, *99*, 15215.